Feshbach-type resonances for two-particle scattering in graphene

C. Gaul,[1,2] F. Domínguez-Adame,[1] F. Sols,[1] and I. Zapata[1,3]
[1]*Departamento Física de Materiales, Universidad Complutense de Madrid, E-28040 Madrid, Spain*
[2]*Max Planck Institute for the Physics of Complex Systems, 01187 Dresden, Germany*
[3]*Departamento Física de la Materia Condensada C-3, Universidad Autónoma de Madrid, E-28049 Madrid, Spain*
(Received 17 July 2013; revised manuscript received 10 December 2013; published 21 January 2014)

Two-particle scattering in graphene is a multichannel problem, where the energies of the identical or opposite-helicity channels lie in disjoint energy segments. Due to the absence of Galilean invariance, these segments depend on the total momentum Q. The dispersion relations for the two opposite-helicity scattering channels are analogous to those of two one-dimensional tight-binding lattices with opposite dispersion relations, which are known to easily bind states at their edges. When an s-wave separable interaction potential is assumed, those bound states reveal themselves as three Feshbach resonances in the identical-helicity channel. In the limit $Q \to 0$, one of the resonances survives and the opposite-helicity scattering amplitudes vanish.

DOI: 10.1103/PhysRevB.89.045420 PACS number(s): 72.80.Vp, 71.10.Li, 72.10.−d

I. INTRODUCTION

Since the advent of graphene [1], whose low-energy excitations behave as massless and chiral Dirac fermions propagating in two dimensions [2,3], the role of electron-electron interactions has been an active research field [4]. In this context, the two-body problem in a single layer of graphene has been studied recently [5,6]. Reference [5] found that, due to the relativistic dispersion relation of electrons in graphene, the conventional decoupling of center-of-momentum and relative coordinates fails, which prevents a simple effective one-body description. The general case of nonzero total momentum was barely addressed in Ref. [5] despite its potential importance for charge transport phenomena in graphene [7]. The main goal of our present work is to contribute to fill this gap by carrying out a detailed analysis of the two-particle scattering problem at nonzero total momentum. Like the work of Refs. [5,6], the study presented here could provide important insights on the many-body physics of graphene.

One aspect of the two-body Dirac scattering in two dimensions which has so far received little attention is its multichannel character. A remarkable feature of multichannel scattering of particles with internal structure is the occurrence of Fano-Feshbach resonances [8–10], extensively studied in nuclear and atomic physics and with a wealth of recent applications to quantum gases [11,12]. In this work we show that similar resonances appear for the two-body problem in graphene.

II. TWO-BODY PROBLEM IN GRAPHENE

We consider the scattering of two interacting particles moving in a perfect graphene lattice. If their crystal momenta are close enough to the same Dirac point, a continuum description in a single valley suffices. Then, the wave function $\Phi_{\alpha\beta}(\mathbf{r}_1,\mathbf{r}_2)$ for two particles has four components, the double index α,β referring to the sublattice (pseudospin) indices of particles 1 and 2 respectively. At energy ϵ, $\Phi_{\alpha\beta}$ is governed by the Dirac equation (we use units in which $\hbar = v_F = 1$)

$$\epsilon\Phi_{\alpha\beta} = -i\boldsymbol{\sigma}_{\alpha\alpha'}\cdot\boldsymbol{\nabla}_1\Phi_{\alpha'\beta} - i\boldsymbol{\sigma}_{\beta\beta'}\cdot\boldsymbol{\nabla}_2\Phi_{\alpha\beta'} + V\Phi_{\alpha\beta}, \quad (1)$$

where doubly appearing indices α' and β' are summed over. The two-dimensional gradient $\boldsymbol{\nabla}_j$ acts on the coordinate of particle j, $\boldsymbol{\sigma}$ is the vector of Pauli matrices, and $V = V(\mathbf{r}_1 - \mathbf{r}_2)$ is the two-body interaction.

Since Eq. (1) conserves the total momentum $\mathbf{Q}$ (measured with respect to the Dirac point), we choose to write the wave function as follows:

$$\Phi_{\alpha\beta}(\mathbf{r}_1,\mathbf{r}_2) = e^{i[\mathbf{Q}\cdot(\mathbf{r}_1+\mathbf{r}_2)/2-\epsilon t]}\Psi_{\alpha\beta}(\mathbf{r}_1-\mathbf{r}_2). \quad (2)$$

As the center-of-mass and relative motions of two particles in a graphene lattice do not factorize [5], the relative wave function $\Psi_{\alpha\beta}(\mathbf{r}_1-\mathbf{r}_2)$ depends on the total momentum $\mathbf{Q}$, which appears as a parameter in the relative two-body problem.

The Fourier transform of the relative wave function is the four-component vector $\Psi(\mathbf{q})$, where $\mathbf{q}$ is half the relative momentum, hereafter expressed in complex notation ($\mathbf{q} \to q \in \mathbb{C}$ and $\mathbf{Q} \to Q \in \mathbb{R}^+$ without loss of generality). In the helicity representation (see Appendix A), the Dirac equation (1) reads

$$\epsilon\Psi(q) = \mathsf{K}(q)\Psi(q) + \frac{1}{\Omega}\sum_{q'} V(q,q')\,\mathsf{U}^\dagger(q)\mathsf{U}(q')\Psi(q'), \quad (3)$$

where Ω is the area. The 4×4 matrices $\mathsf{K}(q)$ and $\mathsf{U}(q)$ are implicit functions of the total momentum Q. We choose to work in the valley where energy and helicity have the same sign. The kinetic energy $\mathsf{K}(q)$ is given by the diagonal matrix

$$\mathsf{K}(q) = \begin{bmatrix} |q_+|+|q_-| & & & \\ & |q_+|-|q_-| & & \\ & & -|q_+|+|q_-| & \\ & & & -|q_+|-|q_-| \end{bmatrix}, \quad (4)$$

with $q_\pm = Q/2 \pm q$ the momentum of the electrons, where we use units $\hbar = v_F = 1$. The unitary matrix $\mathsf{U}(q) = \mathsf{U}_d(q)\mathsf{R}^\dagger$ is related to the transformation from sublattice coordinates to helicities and consists in

$$\mathsf{U}_d(q) = \exp(-i\theta_+\sigma^3/2)\otimes\exp(-i\theta_-\sigma^3/2),$$
$$\mathsf{R} = \exp(-i\pi\sigma^2/4)\otimes\exp(-i\pi\sigma^2/4), \quad (5)$$

σ^i being the Pauli matrices and $\theta_\pm = \arg(q_\pm)$. Finally, $V(q,q')$ is the interaction matrix element for the two-particle scattering process. It is independent of Q and the helicity indices.

The kinetic energy ϵ lies in three nonoverlapping intervals for the four possible helicity channels: $(-\infty,-Q)$ for channel $(--)$, $(-Q,Q)$ for channels $(+-),(-+)$, and (Q,∞) for channel $(++)$. Thus, the elastic collision of two electrons in graphene poses a multichannel problem, with the important peculiarity that, unlike in atomic multichannel scattering, open channels close when energy crosses thresholds. We note that, in the isotropic limit, $Q \to 0$, the central energy interval collapses to a point at $\epsilon = 0$, which results in a nontrivial scattering problem.

Because the two opposite-helicity channels have a bounded energy range, we expect that resonances may appear in the $(--)$ or $(++)$ channels ($|\epsilon| > Q$). These resonances are due to virtual transitions into quasibound states of the $(+-),(-+)$ channels ($|\epsilon| < Q$), which would be true bound states in the absence of coupling between channels. This is the same mechanism which underlies Fano-Feshbach resonances in atomic and nuclear physics. What is unique to the resonances encountered here is the absence of particle internal structure and the fundamental sensitivity to the absolute motion.

A. Symmetries

Negative and positive energies are related by a simple symmetry operation. Consider the matrix $\mathsf{m}_1 = \sigma^1 \otimes \sigma^1$, which interchanges the helicities of both particles. It commutes with $\mathsf{U}^\dagger(q)\mathsf{U}(q')$ and anticommutes with $\mathsf{K}(q)$ in Eq. (3). Thus, applying the transformation m_1 and changing the sign of the interaction $V(q,q')$ is equivalent to changing the sign of the energy. Thus, we may restrict ourselves to positive energies in the rest of this work.

The present problem lacks parity, rotation, and time-reversal symmetry. However, we identify two relevant symmetries:

(i) Permutation of the two colliding particles P_{12}. This exchange operator can be written as $\mathsf{P}_{12} = \hat{P}\mathsf{m}_{12}$, where $\hat{P}q\hat{P} = -q$, and m_{12} interchanges the pseudospin components and (because $[\mathsf{m}_{12},\mathsf{R}] = 0$) helicities $(+-) \leftrightarrow (-+)$. It is easy to prove that $[\mathsf{P}_{12},\mathsf{K}] = [\mathsf{P}_{12},\mathsf{U}] = 0$. Therefore, if the interaction has the symmetry $V(q,q') = V(-q,-q')$, then P_{12} commutes with the Hamiltonian.

(ii) Reflection at the x axis $\mathsf{P}_x = \hat{P}_x\mathsf{m}_3$, where $\hat{P}_x q \hat{P}_x = q^*$, and $\mathsf{m}_3 = \sigma^3 \otimes \sigma^3$. If $V(q,q') = V(q^*,q'^*)$, then P_x commutes with the Hamiltonian.

We will classify the scattering states according to these symmetries later.

B. T-matrix equation and solution

We consider a purely s-wave separable potential $V(q,q') = \lambda_0$ hereafter, such that both symmetries are fulfilled. We will find that even in this simple case, the scattering amplitude displays a rich structure. The T-matrix equation for the two-body scattering problem formulated in Eq. (3) satisfies

$$\mathsf{T}(z;q_f,q_i) = \mathsf{W}(q_f,q_i) + \frac{1}{\Omega}\sum_q \mathsf{W}(q_f,q)\mathsf{G}_0(z;q)\mathsf{T}(z;q,q_i), \tag{6}$$

where $\mathsf{W}(q,q') = \lambda_0\mathsf{U}^\dagger(q)\mathsf{U}(q')$ incorporates interaction and pseudospin rotation, and $\mathsf{G}_0(z;q) = (z-\mathsf{K})^{-1}$ is the unperturbed propagator. Introducing an upper cutoff p_c, the solution of Eq. (6) is

$$\mathsf{T}(z;q_f,q_i) = \mathsf{U}^\dagger(q_f)\left[\lambda_0^{-1} - \mathsf{M}(z)\right]^{-1}\mathsf{U}(q_i), \tag{7}$$

with

$$\mathsf{M}(z) = \frac{1}{4\pi^2}\int_{|q|<p_c} d^2q\, \mathsf{U}(q)\mathsf{G}_0(z;q)\mathsf{U}^\dagger(q).$$

Note that, thanks to the separable s-wave potential, this solution is *exact*.

III. RESULTS

In the q plane, the curves of constant kinetic energy are either homofocal ellipses [channels $(++)$ and $(--)$, for $|\epsilon| > Q$] or homofocal hyperbolae [channels $(+-)$ and $(-+)$, for $|\epsilon| < Q$], which cross at right angles. This suggests the use of elliptic coordinates (see Appendix C). Specifically, the transformation $q = (Q/2)\cosh(u+iv)$, with $u \geqslant 0$ and $-\pi < v \leqslant \pi$, renders the kinetic energy separable,

$$\mathsf{K}(q) = Q\begin{bmatrix}\cosh u & & & \\ & \cos v & & \\ & & -\cos v & \\ & & & -\cosh u\end{bmatrix}. \tag{8}$$

The v dependence of the kinetic energy in the two central channels $(+-),(-+)$ resembles the dispersion relation of a Bloch wave in a tight-binding chain with nearest-neighbor hopping and v playing the role of crystal momentum. In this picture, we would expect the interaction V to play the role of an impurity potential that can nucleate bound states lying outside the band $(-Q,Q)$, where they become resonances for the outer $(--,++)$ channels with incoming energy $|\epsilon| > Q$. Mathematically, this translates into the appearance of poles for the outer-channel propagators in the lower part of the complex-energy plane, and hence in the z dependence of the T matrix (7).

The matrix $\mathsf{M}(z)$ in Eq. (7) can be computed by introducing elliptic coordinates. It becomes of the form

$$\mathsf{M} = \begin{bmatrix}\mathsf{A} & \mathsf{B} \\ \mathsf{B}^\intercal & \mathsf{A}\end{bmatrix}, \quad \mathsf{A} = \begin{bmatrix}d & a \\ a & d\end{bmatrix}, \quad \mathsf{B} = \begin{bmatrix}a & b \\ c & a\end{bmatrix}, \tag{9}$$

where a,b,c,d are complex functions of z, Q, and p_c and are given in Appendix C. The matrix $\mathsf{M}(z)$ inherits the symmetries P_{12} and P_x of the scattering problem Eq. (3): $\mathsf{M}(z)$ commutes with both m_{12} and $\mathsf{m}_1 = \mathsf{R}^\dagger\mathsf{m}_3\mathsf{R} = \sigma^1 \otimes \sigma^1$. The eigenvectors can be classified as symmetric and antisymmetric under m_{12} and m_1, which defines corresponding eigenspaces of the T matrix Eq. (7) (with respect to P_{12} and P_x). In the antisymmetric eigenspace of m_1, two eigenvectors $v_a^\intercal = (0,1,-1,0)/\sqrt{2}$ and $v_s^\intercal = (1,0,0,-1)/\sqrt{2}$ of $\mathsf{M}(z)$ with eigenvalues $d(z) - c(z)$ and $d(z) - b(z)$ are found which are antisymmetric and symmetric under m_{12}, respectively. In the symmetric eigenspace of m_1, two eigenvectors of the form $v_{s\pm}^\intercal(z) = [a_\pm(z),\pm b_\pm(z),\pm b_\pm(z),a_\pm(z)]$ are found, both being also symmetric under m_{12}. All eigenvectors are normalized as $v_i^\intercal(z)v_j(z) = \delta_{ij}$. The explicit formulas for $a_\pm/b_\pm$ are given in

Appendix C. In the basis of eigenstates of m_{12} and m_1, we can write

$$\left[\lambda_0^{-1} - \mathsf{M}(z)\right]^{-1} = \sum_{j=a,s,s\pm} t_j(z) v_j(z) v_j^{\mathsf{T}}(z). \tag{10}$$

The eigenvalues of the T matrix, $t_j(z)$, are functions of a,b,c,d and can be calculated to be

$$\frac{1}{t_a(z)} = \frac{1}{\lambda_0} + \frac{Q}{8\pi} h(x) g(x), \tag{11a}$$

$$\frac{1}{t_s(z)} = \frac{1}{\lambda_0} + \frac{Q}{4\pi}\left[\Gamma_c^2 \rho(x) + \frac{1}{4} h(x) g(x)\right], \tag{11b}$$

$$\frac{1}{t_{s\pm}(z)} = \frac{1}{\lambda_0} + \frac{Q}{8\pi}\left[\Gamma_c^2 \frac{\rho(x)(x \mp \sqrt{x^2+3}) - 1}{h(x)} + \frac{1}{4} h_\pm(x) g(x)\right], \tag{11c}$$

where $x = z/Q$, $h(x) = \sqrt{x^2-1}$, $g(x) = \ln(4\Gamma_c) - \ln[x + h(x)] + i(\pi/2)\,\mathrm{sgn}[\mathrm{Im}(x)]$, $\Gamma_c = p_c/Q$, $\rho(x) = h(x) - x$, and finally

$$h_\pm(x) = \frac{1}{h(x)}\left[x^2 + 1 \pm \frac{h(x) + x[3 + x(2+x^2)\rho(x)]}{\sqrt{x^4 + 2x^2 - 3}\,\rho(x)}\right].$$

For $|x| < 1$, the usual analytical continuation $\sqrt{x^2-1} \to i\sqrt{1-x^2}$ is implied. For $t_{s\pm}(z)$, we have shown only the leading behavior in the cutoff, which is sufficient for the low-energy region considered here.

To compute the scattering amplitudes, we must consider on-shell expressions, thus letting $z = \epsilon + i0^+$ where the dependence of ϵ on the initial and final momenta is channel specific. For example, for $(++)$ scattering one has $\epsilon = |q_+^i| + |q_-^i| = |q_+^f| + |q_-^f|$.

A. Nonresonant scattering

Due to the quadratic dependence on the cutoff of t_s^{-1} and $t_{s\pm}^{-1}$, for most energies within the relevant region $\epsilon \ll p_c$ the collision will be dominated by the antisymmetric (in P_{12}) element alone, $|t_a| \gg |t_{s\pm}|, |t_s|$. By using Eq. (11a) and the projector element from Eq. (D1), we can derive the final formula for the scattering amplitude for two particles colliding in the antisymmetric mode of the $(++)$ incoming channel,

$$T_{++,++}(\epsilon + i0^+; q_f, q_i) = \frac{1}{2}\frac{\sin[(\theta_-^f - \theta_+^f)/2]\sin[(\theta_-^i - \theta_+^i)/2]}{\lambda_0^{-1} + \frac{1}{8\pi}\sqrt{\epsilon^2 - Q^2}\left(\ln\frac{4p_c}{\epsilon + \sqrt{\epsilon^2 - Q^2}} + i\frac{\pi}{2}\right)}. \tag{12}$$

B. Feshbach resonances

As can be guessed from Eq. (11), the symmetric diagonal T-matrix elements are relevant only when the real part of their inverses is very small, $\mathrm{Re}[t_j(z)^{-1}] \simeq 0$. However, for the $(+-)$ and $(-+)$ channels ($|x| < 1$), because in that case $\mathrm{Im}[t_j(z)^{-1}]$ scales with p_c^2 and thus is always large, the symmetric T-matrix element will be very small. By contrast, for the two ($|x| > 1$) channels [$(++)$ if $\lambda_0 > 0$ and $(--)$ if $\lambda_0 < 0$], the possibility of a sharp resonance exists since $\mathrm{Im}[g(z)]$ is small and independent of p_c.

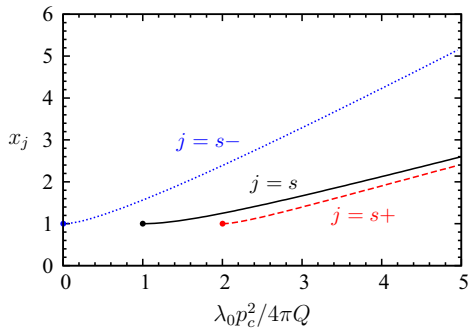

FIG. 1. (Color online) Location of the (asymmetric) resonances Eq. (11), defined by the condition $\mathrm{Re}[t_j(x_j Q)^{-1}] = 0$.

It follows from Eq. (11) that, by just taking into account the dominant quadratic dependence on the cutoff, the equation $\mathrm{Re}[t_s(z_s)^{-1}] = 0$ can be satisfied at $x_s \equiv \epsilon_s/Q$ if

$$\lambda_0 p_c^2 / 4\pi Q = -1/\rho(x_s). \tag{13a}$$

Similarly, in the case of $t_{s\pm}(z)$ given by Eq. (11c), the location of the resonance is given by

$$\frac{\lambda_0 p_c^2}{4\pi Q} = \frac{2\sqrt{x_{s\pm}^2 - 1}}{1 - \rho(x_{s\pm})\left(x_{s\pm} \mp \sqrt{3 + x_{s\pm}^2}\right)}. \tag{13b}$$

As shown in Fig. 1, the solutions x_j of Eqs. (13) are monotonically growing, positive functions of $\lambda_0 p_c^2/4\pi Q$ that start at 0, 1, 2, for $j = s-$, s, and $s+$, respectively. Consequently, the interaction strength $\lambda_0 p_c^2/4\pi Q$ must equal or exceed the thresholds $c_{s-} = 0$, $c_s = 1$, and $c_{s+} = 2$ for the corresponding resonances to occur. The asymptotics for $x_j \gg 1$ are

$$x_j \simeq b_j \frac{\lambda_0 p_c^2}{4\pi Q}, \quad b_{s-} = 1, \quad b_s = b_{s+} = \frac{1}{2}. \tag{14}$$

Thus, for the resonance to occur and the resulting resonance energy to lie in the region where the approximations are valid ($\epsilon_j \ll p_c$), the following condition is necessary and sufficient:

$$c_j b_j \frac{Q}{p_c} < b_j \frac{\lambda_0 p_c}{4\pi} \ll 1. \tag{15}$$

In this situation the inclusion of the other subdominant real part only shifts the position of the resonance by a negligible amount. By Taylor expanding $t_j(z)^{-1}$ near the resonance, one arrives at a Breit-Wigner form,

$$t_j(z) \approx \sqrt{\frac{W_j \Gamma_j}{2\pi}} \frac{1}{z - \epsilon_j + i\Gamma_j/2}, \quad j = s, s+, s-, \tag{16}$$

with weight W_j and width Γ_j. For $j = s$, the results are rather simple, $\Gamma_s \simeq \lambda_0(\epsilon_s^2 - Q^2)/16$ and $W_s \simeq 32\pi\lambda_0$. The ratio $\Gamma_s/\epsilon_s < \lambda_0\epsilon_s/16 \ll 1$ is very small, implying a narrow resonance. For $j = s\pm$, the formulas are lengthy. From their width shown in Fig. 2(a) (along that of $j = s$) one concludes that the Breit-Wigner form survives; hence they are narrow as well. The weight of all resonances are shown in Fig. 2(b).

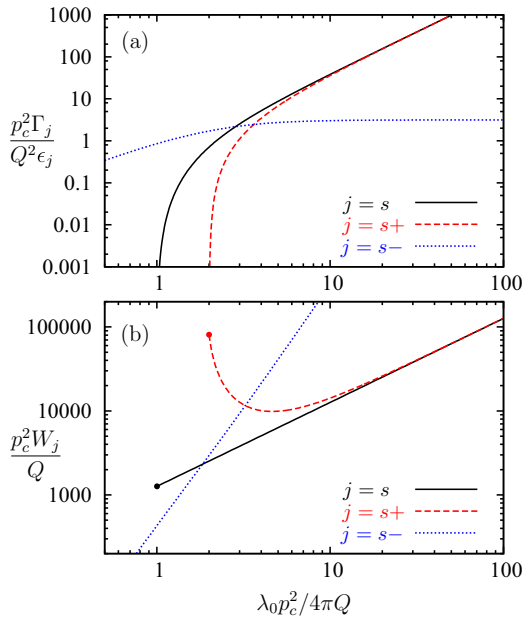

FIG. 2. (Color online) Width Γ_j and weight W_j of the symmetric resonances, defined via $2\pi|t_j(z)|^2 = W_j\Gamma_j/[(z-\epsilon_j)^2+\Gamma_j^2/4]$, for repulsive interaction $\lambda_0 > 0$. The relative width Γ_j/ϵ_j shown in (a) is measured in units of $\Gamma_c^{-2} \ll 1$, i.e., the resonances are always narrow.

The contribution of the resonance s to the scattering amplitude near the resonance reads

$$T_{++,++}(\epsilon + i0^+; q_f, q_i) \simeq \tfrac{1}{2}\, t_s(\epsilon)\sin[(\theta_-^f + \theta_+^f)/2]\sin[(\theta_-^i + \theta_+^i)/2]. \quad (17)$$

The expressions for the other two resonances $s\pm$ are much more involved.

The fact that these resonances are of the Fano-Feshbach type is confirmed by a simple computation in which one neglects the coupling between channels. Then, precisely at the energy given in Eq. (13a), one finds a bound state for the symmetric $(+-)$ and $(-+)$ channel. Once the interchannel coupling is included, this bound state turns into a sharp resonance. This is exactly the same mechanism underlying the appearance of Fano-Feshbach resonances. Close to the resonance energy, the incoming particle pair, say, in the symmetric subspace of the $(++)$ channel with $\lambda_0 > 0$, virtually jumps into the quasibound state in the symmetric subspace of the $(+-)$ and $(-+)$ channels. However, unlike in atomic Fano-Feshbach resonances, the neglect of interchannel coupling is not a good approximation in the present problem mostly because of the locality of the interaction, which strongly mixes the channels. This explains why the other two resonances are not obtained from the same type of reasoning.

The present approach makes a poor prediction about the resonant energies because of their strong dependence on the cutoff. In fact, for this model $\lambda_0 p_c^2/4\pi = \pi V_0$, where V_0 is the interaction at the origin in real space. We can restore units to show that the dimensionless parameter which controls all the characteristics of the resonances is nothing but the ratio of energies $\pi V_0/\hbar v_F Q$. On the other hand, the relative characteristics of the resonances can be shown to be insensitive to variations in the high-momentum content of the interaction if restricted to be of the form $V(q,q') = \lambda_0 f(|q|) f^*(|q'|)$. Specifically, it can be proven that Eqs. (13) remain valid provided that p_c^2 is replaced by a single function of an effective momentum cutoff. This means that for this restricted set of interactions, once a resonance is given, the properties of the other two are independent not only of the cutoff but also of the other model parameters. One could object that total momentum is not strictly conserved for separable interactions. However, momentum conservation does not have to be conserved beyond the Dirac approximation, when umklapp processes in the electron interaction as well as finite bandwidth effects are taken into account.

C. Isotropic limit

The isotropic limit for the $(++)$ channel can be obtained immediately from the previous formulas. One has to remember that in this limit, $\theta_+ - \theta_- \to \pi$, and we take $\epsilon \gg Q$. Some degeneracy of the T matrix must be taken into account but the calculation is otherwise straightforward. We give here the result for the scattering amplitude of two particles colliding in the $(++)$ channel:

$$T_{++,++}(\epsilon + i0^+; q_f, q_i) = \frac{1}{2}\left[\frac{1}{\lambda_0^{-1} + \frac{\epsilon}{8\pi}\left(\ln\frac{2p_c}{\epsilon} + i\frac{\pi}{2}\right)} + \frac{\cos(\alpha_f - \alpha_i)}{\lambda_0^{-1} - \frac{p_c^2}{8\pi\epsilon} + \frac{z}{16\pi}\left(\ln\frac{2p_c}{\epsilon} + i\frac{\pi}{2}\right)}\right], \quad (18)$$

where $\alpha_{i,f} \equiv \arg(q_{i,f})$.

The first term is similar to that encountered in the one-body scattering by an impurity (see Appendix B), with a smooth behavior as a function of energy. By contrast, the second term is specific of two-body scattering and displays a sharp resonance provided the second condition in Eq. (15) is fulfilled. The well defined limits for the position and the width of the resonance are $\epsilon_r \simeq \lambda_0 p_c^2/8\pi$ and $\Gamma \simeq \lambda_0 \epsilon_r^2/16$.

On the other hand, the isotropic limit in the $(+-)$-$(-+)$ channels is more delicate. As the kinetic energy range collapses to a point, we have to use a different approach. Here we fix the incoming momenta and let $Q \to 0$. This implies that the energy has to vanish as well, with $\epsilon \sim Q\cos\alpha_i$ and $q_i = |q_i|\exp(i\alpha_i)$. This implies that $\cos\alpha_f = \pm\cos\alpha_i$ because of the possible helicity flip, but there is no restriction on $|q_f|$.

The leading behavior for the scattering amplitudes in these channels is $t_a(\epsilon) \sim Q^2$ while $t_s(\epsilon)$ and $t_{s\pm}(\epsilon)$ scale as Q/p_c^2, which clearly shows that scattering amplitudes vanish in this isotropic limit (see Appendix E). A possible explanation for this fact relies again on the analogy with the tight-binding Hamiltonian. The $Q \to 0$ limit can be seen as the limit in which the width of the band becomes very narrow. The effective mass of the tight-binding particles increases without limit, meaning that any state prepared with a given lattice momentum q_i will suffer very little scattering.

IV. CONCLUSIONS

We have identified an analogy between the two-particle scattering in graphene and the Fano-Feshbach effect in atomic

and nuclear physics. As an example, the case of an s-wave separable potential has been fully analyzed. A set of resonances has been found whose origin is traced back to virtual transitions into closed channels. Our study establishes a connection between the fields of electronic interactions in graphene and Fano-Feshbach resonances in cold atom systems.

ACKNOWLEDGMENTS

The authors thank F. Guinea and N. Zinner for helpful comments. This work was supported by MINECO through Grants No. FIS2010-21372 and No. MAT2010-17180, by Comunidad de Madrid through Grant Microseres-CM, and by the EU through Marie Curie ITN NanoCTM. Research of C.G. was supported by a PICATA postdoctoral fellowship from the Moncloa Campus of International Excellence (UCM-UPM).

APPENDIX A: DIRAC EQUATION IN GRAPHENE

Free Dirac equation. We use units in which $\hbar = v_F = 1$ and the Einstein summation convention on repeated indexes, unless the repeated index appear at both sides of the equation, being orphaned in only one of the sides. Indexes given by the first letters of the Greek alphabet, $\alpha,\beta,\ldots = \uparrow,\downarrow$, refer to pseudospin (sublattice quantum number), those with Latin letters, $j,k = 1,2 \equiv x,y$, will run in two-dimensional Euclidean space and those with late letters of the Greek alphabet, $\sigma,\tau,\ldots = +,-$, refer to the helicity of the particle. The single-valley one-particle Dirac equation in graphene in real space reads

$$i\,\partial_t \psi_\alpha(\mathbf{r},t) = -i\,\partial_j \sigma^j_{\alpha\beta}\psi_\beta(\mathbf{r},t) + V(\mathbf{r})\psi_\alpha(\mathbf{r},t), \tag{A1}$$

where $\mathbf{r} = (x,y)$ and σ^j, $j = 1,2,3$ denote the Pauli matrices.

When $V(\mathbf{r}) = 0$, the plane-wave solutions can be chosen as $\psi_\alpha(\mathbf{r},t) \sim \mathsf{w}_{\alpha\sigma}(\mathbf{k})\, e^{i(\mathbf{k}\cdot\mathbf{r}-\epsilon t)}$, where $\mathbf{k}$ is the momentum and $\epsilon = \sigma|\mathbf{k}|$ is the energy. The columns of $\mathsf{w}(\mathbf{k})$ are normalized spinors and satisfy

$$k_j \sigma^j_{\alpha\beta}\mathsf{w}_{\beta\sigma}(\mathbf{k}) = \sigma k\, \mathsf{w}_{\alpha\sigma}(\mathbf{k}). \tag{A2}$$

Orthonormality and completeness for the spinors read $\mathsf{w}^\dagger(\mathbf{k})\,\mathsf{w}(\mathbf{k}) = \mathsf{w}(\mathbf{k})\,\mathsf{w}^\dagger(\mathbf{k}) = \mathsf{1}$. Specifically, we chose the spinors as in Ref. [3]:

$$\mathsf{w}(\mathbf{k}) = \frac{1}{\sqrt{2}}\begin{pmatrix} e^{-i\theta_k/2} & e^{-i\theta_k/2} \\ e^{i\theta_k/2} & -e^{-i\theta_k/2}\end{pmatrix}, \tag{A3}$$

with $\mathbf{k} = k\,(\cos\theta_k, \sin\theta_k)$. For later use we collect some useful formulas here,

$$\mathsf{w}^\dagger(\mathbf{k_1})\,\mathsf{w}(\mathbf{k_2}) = e^{i(\theta_1-\theta_2)\sigma^1/2} = \mathsf{u}^\dagger(\mathbf{k_1})\,\mathsf{u}(\mathbf{k_2}),$$

$$\mathsf{u}(\mathbf{k}) = \mathsf{w}(\mathbf{k})\sigma^1 = e^{-i\theta_k\sigma^3/2}\, e^{i\pi\sigma^2/4} = \mathsf{u}_d(\mathbf{k})\,\mathsf{r}^\dagger.$$

Normalized solutions of the one-particle Dirac equation will be written in real and Fourier spaces, and helicity or pseudospin basis, as

$$\begin{aligned}
\psi_\alpha(\mathbf{k},t) &= \mathsf{w}_{\alpha\sigma}(\mathbf{k})\,\psi_\sigma(\mathbf{k},t) = \frac{1}{\sqrt{\Omega}}\int_\Omega d^2r\,\psi_\alpha(\mathbf{r},t)\,e^{-i\mathbf{k}\cdot\mathbf{r}}, \\
\psi_\sigma(\mathbf{k},t) &= \mathsf{w}^\dagger_{\sigma\alpha}(\mathbf{k})\,\psi_\alpha(\mathbf{k},t), \\
\psi_\alpha(\mathbf{r},t) &= \frac{1}{\sqrt{\Omega}}\sum_k \psi_\alpha(\mathbf{k},t)\,e^{i\mathbf{k}\cdot\mathbf{r}}.
\end{aligned} \tag{A4}$$

Interaction potential. The potential $V(r)$ is assumed to be spherically symmetric and short ranged. The Fourier transform reads

$$\begin{aligned}
V(\mathbf{k},\mathbf{q}) &= \int_\Omega d^2r\, e^{-i(\mathbf{k}-\mathbf{q})\cdot\mathbf{r}} V(r) \\
&= \sum_{l=-\infty}^{\infty} e^{il(\theta_q-\theta_k)} V_l(k,q),
\end{aligned} \tag{A5}$$

with

$$V_l(k,q) = 2\pi\int_0^\infty dr\, r\, V(r)\, J_l(kr)\, J_l(qr),$$

where $J_n(z)$ is the Bessel function of integer order. A separable s-wave approximation, which dominates low-energy scattering, is used through out this work $V_l(k,q) \simeq \lambda_l k^l q^l$, namely $V(\mathbf{k},\mathbf{q}) \simeq \lambda_0$. This approach is valid for $k,q \ll 1/a$, a being the range of the potential. Therefore, the action of the potential on the wave function $V(r)\psi(\mathbf{r})$ is expressed in momentum space as $(1/\Omega)\sum_q \lambda_0\psi(\mathbf{q})$ within this approximation.

APPENDIX B: SCATTERING BY A SEPARABLE s-WAVE IMPURITY

Here we solve the scattering problem for a single electron at very low energies using the s-wave separable approximation. The obtained T matrix shows the leading behavior at low energies for short-range impurities. We start from (A1), as written in momentum space and then transformed to helicities. For a separable potential the result is

$$\begin{aligned}
i\,\partial_t\psi_\sigma(\mathbf{k},t) = \sigma k\psi_\sigma(\mathbf{k},t) &+ \frac{\lambda_0}{\Omega}(e^{i\theta_k\sigma^1/2})_{\sigma\sigma'} \\
&\times \sum_q (e^{-i\theta_q\sigma^1/2})_{\sigma'\tau}\psi_\tau(\mathbf{q},t).
\end{aligned} \tag{B1}$$

The corresponding T-matrix equation will be written as

$$\begin{aligned}
\mathsf{T}(z;\mathbf{k}_1,\mathbf{k}_2) &= \lambda_0\, e^{i(\theta_{k_1}-\theta_{k_2})\sigma^1/2} \\
&+ \frac{1}{\Omega}\sum_q \mathsf{W}(\mathbf{k}_1,\mathbf{q})\mathsf{G}_0(z;\mathbf{q})\mathsf{T}(z;\mathbf{q},\mathbf{k}_2),
\end{aligned} \tag{B2}$$

where $\mathsf{G}_0(z;\mathbf{q})$ is the diagonal propagator, whose elements are given by $1/(z-\sigma q)$.

The solution to (B2) for an s-wave separable potential can be sought in the form $\mathsf{T}(z;\mathbf{k},\mathbf{q}) = e^{i\theta_k\sigma^1/2}\mathsf{T}(z)\,e^{-i\theta_q\sigma^1/2}$ where, after substitution of this ansatz in (B2) and solving for $\mathsf{T}(z)$, we get the solution $\mathsf{T}(z) = [\lambda_0^{-1} - \mathsf{M}(z)]^{-1}$ with

$$\mathsf{M}(z) = \frac{1}{(2\pi)^2}\int_{-\pi}^{\pi} d\theta e^{-i\theta\sigma^1/2}\left[\int_0^{p_c} dk\, k\, \mathsf{G}_0(z;\mathbf{k})\right] e^{i\theta\sigma^1/2},$$

where p_c is a cutoff on the order of the smallest of the inverse of potential range $1/a$ or the inverse of the lattice spacing $1/b$. When $|z| \ll p_c$, $\mathrm{Re}(z) > 0, \mathrm{Im}(z) > 0$ the solution for the full T matrix is found to be

$$\mathsf{T}(z;\mathbf{k}_1,\mathbf{k}_2) = \frac{1}{\lambda_0^{-1} - \frac{z}{2\pi}\left[\ln\frac{z}{p_c} - i\frac{\pi}{2}\right]}\begin{bmatrix} C_{12} & iS_{12} \\ iS_{12} & C_{12}\end{bmatrix}, \tag{B3}$$

where for brevity we define $C_{12} = \cos(\theta_1/2 - \theta_2/2)$ and $S_{12} = \sin(\theta_1/2 - \theta_2/2)$.

TABLE I. Table of integrals for the evaluation of Eq. (C1). The imaginary parts drop out from the second column and are not shown in the third because they are odd in v. Here we have defined $I_{s2} = \int_0^{u_c} du\, \sinh^2 u = (1/4)[\sinh(2u_c) - 2u_c] \simeq 2p_c^2/Q^2 - u_c/2$, $I_{c2} = \int_0^{u_c} du\, \cosh^2 u = (1/4)[\sinh(2u_c) + 2u_c] \simeq 2p_c^2/Q^2 + u_c/2$, and $I_{c1} = \int_0^{u_c} du\, \cosh u = \sinh u_c = 2p_c/Q$.

(n_+, n_-)	$\int_{-\pi}^{\pi} dv\, \lvert\sinh(u+iv)\rvert^2 \times e^{in_+\theta_+} e^{in_-\theta_-}$	$\int_0^{u_c} du\, \lvert\sinh(u+iv)\rvert^2 \times e^{in_+\theta_+} e^{in_-\theta_-}$
(0,0)	$\pi(2\sinh^2 u + 1)$	$I_{s2} + u_c \sin^2 v$
(0,±1)	$\pi \cosh u$	$-I_{s2}\cos v + I_{c1}\sin^2 v$
(±1,0)	$\pi \cosh u$	$I_{s2}\cos v + I_{c1}\sin^2 v$
(±1,±1)	π	$-I_{c2}\cos(2v) + u_c \cos^2 v$
(±1,∓1)	$-\pi(2\sinh^2 u - 1)$	$-I_{s2} + u_c \sin^2 v$

APPENDIX C: ELLIPTIC COORDINATES

In this Appendix, the momentum $q = q_x + iq_y \in \mathbb{C}$ and we will write explicitly $|q|$ for the modulus. The total momentum is, by convention, real and positive, $Q > 0$. The transformation to elliptic coordinates reads $q = (Q/2)\cosh(u+iv)$ with $u \geqslant 0$ and $-\pi < v \leqslant \pi$ (see Ref. [13]).

All integrals needed in the main text are of the form

$$\int_0^{u_c} du \int_{-\pi}^{\pi} dv \frac{Q^2}{4} |\sinh(u+iv)|^2 e^{in_+\theta_+} e^{in_-\theta_-} \times \left\{ \frac{1}{z \pm Q\cos(v)}, \frac{1}{z \pm Q\cosh(u)} \right\}, \tag{C1}$$

where $n_\pm = 0, -1, 1$ and

$$e^{i\theta_+} = \frac{\cosh\left(\frac{u+iv}{2}\right)}{\cosh\left(\frac{u-iv}{2}\right)}, \quad e^{i\theta_-} = -\frac{\sinh\left(\frac{u+iv}{2}\right)}{\sinh\left(\frac{u-iv}{2}\right)}.$$

The results after integration are collected in Table I. The cutoffs in the different coordinate systems are chosen as $p_c = (Q/2)\sinh u_c$, $u_c \simeq \ln(4p_c/Q)$ and therefore $(1/4)\sinh(2u_c) = 2p_c^2/Q^2 + \mathcal{O}(1)$.

Using Table I, we find the integrals a, b, c, d of the main text as follows:

$$\begin{aligned} a(z) &= \frac{1}{16\pi Q h\left(\frac{z}{Q}\right)}\left[2p_c^2\rho\left(\frac{z}{Q}\right) + \frac{zQ}{2}g\left(\frac{z}{Q}\right)\right], \\ b(z) &= \frac{1}{16\pi Q h\left(\frac{z}{Q}\right)}\left[2p_c^2\rho^2\left(\frac{z}{Q}\right) - \frac{Q^2}{2}g\left(\frac{z}{Q}\right)\right], \\ c(z) &= \frac{1}{16\pi Q h\left(\frac{z}{Q}\right)}\left[2p_c^2 + \left(z^2 - \frac{3Q^2}{2}\right)g\left(\frac{z}{Q}\right)\right], \\ d(z) &= \frac{1}{16\pi Q h\left(\frac{z}{Q}\right)}\left[2p_c^2 - \left(z^2 - \frac{Q^2}{2}\right)g\left(\frac{z}{Q}\right)\right], \end{aligned} \tag{C2}$$

where $\rho(x)$, $h(x)$, and $g(x)$ are defined in the main text after Eq. (11). The leading term in the cutoff is proportional to p_c^2. The function $g(z/Q)$ is a correction of logarithmic order.

The eigenvalues and eigenvectors of the matrix M, which consists of the expressions given in (C2), are given in the main text [before Eq. (10) and in Eqs. (11)], except for the eigenvectors $v_{s\pm}^{\mathsf{T}}(z) = [a_\pm(z), \pm b_\pm(z), \pm b_\pm(z), a_\pm(z)]$. The ratio of the entries reads

$$\frac{a(z)_\pm}{b(z)_\pm} = \frac{b(z)_\mp}{a(z)_\mp} = \sqrt{1 + \frac{c(z)-b(z)}{4|a(z)|}} \pm \frac{c(z)-b(z)}{4|a(z)|}, \tag{C3}$$

where, according to Eqs. (C2), $c(z) - b(z) > 0$ and $a(z) < 0$ for $z > Q$.

APPENDIX D: PROJECTORS FOR s, $s+$, AND $s-$

In Eq. (17) of the main text, we have considered the (++)-(++) component of the asymmetric projector matrix $[\mathsf{U}^\dagger(q) v_a v_a^{\mathsf{T}} \mathsf{U}(q')]_{++,++} \equiv X_a(q,q')$, with the result

$$X_a(q,q') = \frac{1}{2}\sin\left(\frac{\theta_- - \theta_+}{2}\right)\sin\left(\frac{\theta'_- - \theta'_+}{2}\right). \tag{D1}$$

Close to the resonances (see Sec. IIIB), we need also the symmetric projectors. There, we find

$$\begin{aligned} X_s(q,q') &= \frac{1}{2}\sin\left(\frac{\theta_- + \theta_+}{2}\right)\sin\left(\frac{\theta'_- + \theta'_+}{2}\right), \\ X_{s\pm}(q,q') &= \left[a_\pm(z)\cos\left(\frac{\theta_- + \theta_+}{2}\right) \mp b_\pm(z)\cos\left(\frac{\theta_- - \theta_+}{2}\right)\right] \\ &\quad \times \left[a_\pm(z)\cos\left(\frac{\theta'_- + \theta'_+}{2}\right) \mp b_\pm(z)\cos\left(\frac{\theta'_- - \theta'_+}{2}\right)\right], \end{aligned} \tag{D2}$$

where $a_\pm(z)$ and $b_\pm(z)$ are assumed to be normalized such that $2(a_\pm^2 + b_\pm^2) = 1$. In the isotropic limit ($Q \to 0$) the expression $a(z)_+/b(z)_+ = b(z)_-/a(z)_-$ in Eq. (C3) tends to infinity. So, we have $a_+ \to 1/\sqrt{2}$, $b_+ \to 0$, $a_- \to 0$, and $b_- \to 1/\sqrt{2}$, such that the above expression simplifies to

$$X_{s\pm}(q,q') \to \frac{1}{2}\cos\left(\frac{\theta_- \pm \theta_+}{2}\right)\cos\left(\frac{\theta'_- \pm \theta'_+}{2}\right). \tag{D3}$$

APPENDIX E: ISOTROPIC LIMIT $Q \to 0$

(++) *scattering channel*. As discussed in the main text, the isotropic limit for this situation can be obtained by $Q \to 0$ leaving $\epsilon \gg Q$ fixed. This limit is straightforward from Eqs. (11). Rotational symmetry makes the states s,$s-$ degenerate. The space spanned by v_s,v_{s+} has (1,0,0,0) and (0,0,0,1) as basis vectors. The state $s-$ has a very simple spinor, $v_{s-} = (0,1,1,0)/\sqrt{2}$, but it is projected to zero in the (++) channel.

(+−),(−+) *scattering channels*. The limit we consider in this situation is with fixed incoming momenta, so $\epsilon \sim Q\cos(\theta_i)$, being $q_i = |q_i|e^{i\theta_i}$ the incoming momentum. We here make a definite assumption of entrance in (+−) and such that $0 \leqslant \theta_i \leqslant \pi/2$, in order to ease the notation. After a long but straightforward computation, the dominant ($Q \to 0$)

on-shell scattering amplitude elements are found to be

$$t_a = \pm\frac{\lambda_0 Q^2}{2|q_i q_f|}\,\sin(q_i)\sin(q_f), \quad t_s = -\frac{2\pi Q e^{i\theta_i}}{p_c^2}\,\sin(q_i)\sin(q_f),$$
$$t_{s+} = \pm\frac{4\pi Q}{p_c^2 f_+(\theta_i)}, \quad t_{s-} = \frac{4\pi Q}{p_c^2 f_-(\theta_i)}\cos(q_i)\cos(q_f), \tag{E1}$$

with

$$f_\pm(\theta) = \cos(\theta) + i[2\csc(\theta) - \sin(\theta)] \pm i\sqrt{3+\cos^2(\theta)}\csc(\theta)e^{-i\theta},$$

where the sign $\pm$ is chosen according to $\cos(\theta_i) = \pm\cos(\theta_f)$.

[1] K. S. Novoselov, A. K. Geim, S. V. Morozov, D. Jiang, Y. Zhang, S. V. Dubonos, I. V. Grigorieva, and A. A. Firsov, Science **306**, 666 (2004).

[2] P. R. Wallace, Phys. Rev. **71**, 622 (1947).

[3] A. H. Castro Neto, F. Guinea, N. M. R. Peres, K. S. Novoselov, and A. K. Geim, Rev. Mod. Phys. **81**, 109 (2009).

[4] V. Kotov, B. Uchoa, V. Pereira, F. Guinea, and A. Neto, Rev. Mod. Phys. **84**, 1067 (2012).

[5] J. Sabio, F. Sols, and F. Guinea, Phys. Rev. B **81**, 045428 (2010).

[6] R. N. Lee, A. I. Milstein, and I. S. Terekhov, Phys. Rev. B **86**, 035425 (2012).

[7] N. M. R. Peres, Rev. Mod. Phys. **82**, 2673 (2010).

[8] U. Fano, Nuovo Cimento **12**, 154 (1935).

[9] U. Fano, Phys. Rev. **124**, 1866 (1961).

[10] H. Feshbach, Ann. Phys. **5**, 357 (1958).

[11] T. Köhler, K. Góral, and P. Julienne, Rev. Mod. Phys. **78**, 1311 (2006).

[12] C. Chin, R. Grimm, P. Julienne, and E. Tiesinga, Rev. Mod. Phys. **82**, 1225 (2010).

[13] M. Spiegel and J. Liu, *Schaum's Outline of Mathematical Handbook of Formulas and Tables* (Mcgraw-Hill, New York, 1998).